

INVESTIGATION ON THE AERODYNAMIC INSTABILITY OF A SUSPENSION BRIDGE WITH A HEXAGONAL CROSS-SECTION

Fuh-Min Fang*, Yi-Chao Li, Tsung-Chi Liang, and Chu-Chang Chen

ABSTRACT

The aerodynamic instability of a suspension bridge with a hexagonal cross-section is investigated systematically based on a two-dimensional model. Measurements of the dynamic responses of a sectional bridge model in the cross-wind and torsional directions were firstly carried out in a wind tunnel. The results were used to guide and confirm the execution of parallel numerical simulations. Accordingly, both the experimental and numerical results are used as bases to examine the flow effect as well as the aeroelastic behavior of the bridge in detail.

Results show that the numerical predictions of the structural responses agree well with those from the experiments, indicating that the proposed numerical method is capable of predicting the deck motion with good accuracy. Based on the time-series numerical results, extensive investigations reveal that a hexagonal deck has much better aerodynamic stability performance than a rectangular one. Finally, among the hexagonal decks studied, it is found that one with a 30° side angle leads to the greatest critical flutter speed.

Key Words: suspension bridge, numerical computation, section model.

I. INTRODUCTION

The aerodynamic instability of a suspension bridge is generally a major concern in design since a long-span structure is most sensitive to wind. Physically, when wind passes the bridge, which usually possesses a blunt shape, vortex shedding occurs and causes unsteady wind load on the structure. As the extent of the resulting bridge vibration is significant, it can further affect the surrounding flow and promote a structural response. Therefore, the analysis of the interaction between the structure motion and the wind flow become important. In order to investigate the dynamics of the bridge as well as the corresponding wind effects, the method of model experiments is commonly used. Economically,

however, the application of appropriate numerical methods can be another option. Besides, the numerical results can provide more extensive information for the analysis of flow-structure interactive problems.

A number of researchers have investigated, experimentally, the mechanisms of wind-induced vibration of suspension bridges. Typically, Scanlan and Tomko (1971) proposed a semi-experimental and semi-analytical approach regarding flutter derivatives, and this approach is presently widely used. Sarkar *et al.* (1992) suggested a system identification procedure to estimate all the flutter derivatives simultaneously. In their study, numerical simulations and reduction of the experimentally-obtained direct derivatives were presented. Iwamoto and Fujino (1995) proposed a method of simultaneous identification of all eight flutter derivatives of bridge decks from free-vibration data. They showed, by experiments, that an increase of mass and inertial moment of a section model lead to better accuracy in identifying the flutter derivatives at high wind speeds. Additionally, based on the experimental results from a coupled vertical-torsional free vibration of a spring-suspended section model, Gu *et al.* (2000) employed a least-square theory

*Corresponding author. (Tel: 886-4-22851707; Email: fmfang@nchu.edu.tw)

F. M. Fang, Y. C. Li, and T. C. Liang are with the Department of Civil Engineering, National Chung Hsing University, Taichung, Taiwan 402, R.O.C.

C. C. Chen is with the Department of Information Management, Chung Chou Institute of Technology, Changhwa, Taiwan 510, R.O.C.

and proposed an identification method to obtain flutter derivatives. Moreover, Noda *et al.* (2003) evaluated the flutter derivatives of thin rectangular cylinders and found that the effect of oscillation amplitudes could be significant.

Besides wind tunnel model tests, the method of computational fluid dynamics (CFD) has also been used to examine the aerodynamic performance and aeroelastic stability of long-span bridges. Kuroda (1997) presented a numerical simulation of high-Reynolds-number flows past a fixed section model with a shallow hexagonal cross-section. The overall characteristics of measured static force coefficients were well captured by the computations. Lee *et al.* (1997) investigated, numerically, the wind loading characteristics for turbulent flows over a two-dimensional bridge deck cross-section. The two-dimensional flow results were further used to perform three-dimensional dynamic structural analyses on a non-interactive basis. Fang *et al.* (2001) proposed a numerical method to simulate the surrounding wind flow and to predict the corresponding dynamic responses of a bridge deck with a rectangular cross-section. By employing a partially interactive procedure, the dynamic responses of the deck agreed well with the measurement results in a case where torsional responses were relatively insignificant. Furthermore, improvements were made successfully by Fang *et al.* (2005) to analyze the motion of a bridge with a trapezoidal cross-section based on a completely interactive procedure.

In summary, the analytical approach proposed by Scanlan and Tomko (1971) in terms of flutter derivatives provides a method of extensive examination of bridge instability in two-dimensions. Based on this approach, Sarkar *et al.* (1992), Iwamoto and Fujino (1995), Gu *et al.* (2000) and Noda *et al.* (2003) extend the concept into practical bridge instability analyses. Since all these studies were carried out by wind tunnel tests, the analyses were limited to certain selected variables that could technically be measured. Regarding the before-mentioned numerical studies, on the other hand, most of them concentrated on the flow effects of bridge decks. Not much emphasis was put on the interaction between the behavior of the vibrating deck and the surrounding flow. To examine the dynamics involved, it is attempted in this study to analyze the bridge instability problem by using both the methods of wind tunnel measurements and numerical simulations, which allow for investigations on the interaction mechanism in more detail.

II. PROBLEM DESCRIPTION

In the study, a numerical model is proposed to simulate the dynamic response of a suspended bridge

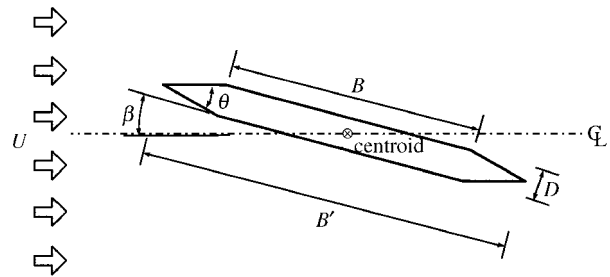


Fig. 1 Sketch of problem

in a two-dimensional sense. Particularly, a bridge deck with a hexagonal cross-section is assessed. In the numerical computations, two sets of equations, one for the simulation of the unsteady surrounding turbulent flow and the other for the calculation of the vibrating motions of the bridge deck, are solved alternately to reflect the interaction effect between the structure and the flow. The resulting time-series responses of the structure as well as the wind loads are analyzed to examine the dynamic behaviors of the two. To verify the accuracy of the numerical results, additional wind tunnel experiments were conducted on a sectional deck model and the results of the vertical and torsional motions of the deck were used to confirm the numerical predictions. Finally, both the experimental and numerical results are used to examine the flow effect as well as the aeroelastic behavior of the bridge in detail.

Figure 1 depicts the schematic of the problem. At five selected attack angles ($\beta = 0^\circ, \pm 4^\circ$ and $\pm 8^\circ$), the approaching flow is considered smooth with a speed (U_o) varying from 2 to about 48 m/s in the numerical predictions and 2 to about 20 m/s in the model experiments. The mass distribution of the bridge cross-section is assumed uniform so that the effect due to eccentricity is not of concern. The hexagonal bridge cross-section is symmetric to the centroid with four side angles ($\theta = 30^\circ, 60^\circ, 90^\circ$ and 180°), corresponding respectively to a total deck width (B') varying from 13.73 to 8.00 times of the deck thickness (D). It is noted that the widths of the upper surfaces (B) in all the deck selections were kept the same ($8D$) to provide a consistent basis for the comparison of the aerodynamic performance among the decks. Particularly, as θ equals to 180° , the shape of the deck cross-section becomes a rectangle. Other related properties of the bridge decks are illustrated in Table 1.

III. NUMERICAL METHOD

The simulations contain two separate computations which are performed according to an interactive procedure. To predict the unsteady turbulent flow around the deck, a weakly-compressible-flow method

Table 1 Related properties of present section model

Side angle (θ)	Aspect ratio (B^*/D)	Mass (M) (kg/m)	Momentum of inertia (I) (kg-m ² /m)	Fundamental frequency (Hz)			Damping ratio (%)	
				Vertical (f_V)	Torsional (f_T)	Frequency ratio (ϵ)	Vertical (ξ_V)	Torsional (ξ_T)
180°	8.00	3.785	1.29×10^{-2}	9.86	20.53	2.08	0.54	0.77
90°	9.00	4.106	1.51×10^{-2}	9.06	18.95	2.09	0.58	0.72
60°	9.73	3.861	1.31×10^{-2}	9.74	20.62	2.12	0.58	0.72
30°	11.73	3.873	1.30×10^{-2}	9.67	20.59	2.13	0.58	0.81

(Song and Yuan, 1988) together with a dynamic subgrid-scale turbulence model (Germano *et al.*, 1991) is applied. After an instantaneous flow field is simulated, the resulting pressure distribution on the deck surfaces is integrated to obtain the wind load, which is taken as an input to further compute the corresponding structure responses. The resulting deflections and the vibrating speeds of the deck are then fed back to the boundary specifications of the deck surfaces for the flow calculations in the following time step. The alternative solutions of the instantaneous flow field and the deck motions in time series are considered the results of the interactive dynamic behaviors of the two.

1. Flow Calculations

In the weakly-compressible-flow method (Song and Yuan, 1988), the continuity and momentum equations are

$$\frac{\partial p}{\partial t} + k \nabla \cdot \mathbf{V} = 0, \tag{1}$$

$$\frac{\partial \mathbf{V}}{\partial t} + \mathbf{V} \cdot \nabla \mathbf{V} = - \nabla \frac{p}{\rho} + \nabla \cdot [(\nu + \nu_t) \nabla \mathbf{V}], \tag{2}$$

where p , \mathbf{V} and t denote respectively pressure, velocity and time; k is the bulk modulus of elasticity of air; ν and ν_t are respectively the laminar and turbulent viscosities. The turbulent viscosity (ν_t) is determined based on a subgrid-scale turbulence model as

$$\nu_t = C_S \Delta^2 \left(\frac{S_{ij}^2}{2}\right)^{0.5}, \tag{3}$$

where C_S is the Smagorinsky coefficient; Δ denotes the characteristic length of the computational grid and $S_{ij} = (\frac{\partial u_j}{\partial x_i} + \frac{\partial u_i}{\partial x_j})$. Based on a concept of dynamic model proposed by Germano *et al.* (1991), two grid systems, corresponding respectively to a grid filter and a test filter, were used in the flow calculations. By comparing the resulting differential turbulent shear stresses associated with the two filter systems at a certain time step in the computation, the C_S value at the next time step is then obtained.

Equations (1) and (2) are further transformed into a coordinate system which goes with the motions of the bridge deck. Accordingly, as the coordinate systems are related by

$$\begin{aligned} X &= x \cos \alpha + y \sin \alpha \\ Y &= y \cos \alpha - x \sin \alpha - \int \dot{y}_V dt \end{aligned} \tag{4}$$

where (X, Y) and (x, y) are the spatial coordinates associated respectively with the new (moving) and the original (fixed) coordinate systems; y_V and α denote the vertical and torsional deflections of the deck; \dot{y}_V , $\dot{\alpha}$, are respectively the corresponding vibration speeds in the vertical (across-wind) and torsional directions, Eqs. (1) and (2) become

$$\begin{aligned} \frac{\partial p}{\partial t} + k [(\frac{\partial u}{\partial X} + \frac{\partial v}{\partial Y}) \cos \alpha + (\frac{\partial u}{\partial Y} - \frac{\partial v}{\partial X}) \sin \alpha] \\ + \frac{\partial p}{\partial X} (-\dot{\alpha} x \sin \alpha - \dot{\alpha} y \cos \alpha) \\ + \frac{\partial p}{\partial Y} (-\dot{\alpha} y \sin \alpha + \dot{\alpha} x \cos \alpha - \dot{y}_V) = 0, \end{aligned} \tag{5}$$

X-direction:

$$\begin{aligned} \frac{\partial u}{\partial t} + (u \frac{\partial u}{\partial X} + v \frac{\partial u}{\partial Y}) \cos \alpha + (u \frac{\partial u}{\partial Y} - v \frac{\partial u}{\partial X}) \sin \alpha \\ + [\frac{\partial u}{\partial X} (-\dot{\alpha} x \sin \alpha - \dot{\alpha} y \cos \alpha) \\ + \frac{\partial u}{\partial Y} (-\dot{\alpha} y \sin \alpha + \dot{\alpha} x \cos \alpha - \dot{y}_V)] \\ = - [\frac{\partial p}{\partial X} \cos \alpha + \frac{\partial p}{\partial Y} \sin \alpha] + (\nu + \nu_t) (\frac{\partial^2 u}{\partial X^2} + \frac{\partial^2 u}{\partial Y^2}) \end{aligned} \tag{6a}$$

Y-direction:

$$\begin{aligned} \frac{\partial v}{\partial t} + (u \frac{\partial v}{\partial X} + v \frac{\partial v}{\partial Y}) \cos \alpha + (u \frac{\partial v}{\partial Y} - v \frac{\partial v}{\partial X}) \sin \alpha \\ + [\frac{\partial v}{\partial X} (-\dot{\alpha} x \sin \alpha - \dot{\alpha} y \cos \alpha) \\ + \frac{\partial v}{\partial Y} (-\dot{\alpha} y \sin \alpha + \dot{\alpha} x \cos \alpha - \dot{y}_V)] \\ = - [\frac{\partial p}{\partial X} (-\sin \alpha) + \frac{\partial p}{\partial Y} \cos \alpha] + (\nu + \nu_t) (\frac{\partial^2 v}{\partial X^2} + \frac{\partial^2 v}{\partial Y^2}). \end{aligned} \tag{6b}$$

Based on Eqs. (5) and (6), the computation of the flow proceeds according to a finite-volume approach with an explicit finite-difference scheme. To ensure numerical stability, the time increment in the unsteady calculations is limited by the Courant-Friedrich-Lewy criterion (Courant *et al.*, 1967).

In the flow calculations, appropriate values of pressures and velocities are specified at exterior (phantom) grids outside the boundaries of the computational domain to reflect the physical nature of the boundaries. For the velocity specifications, since the computation is based on a non-stationary coordinate system, the boundary specifications at the deck surfaces have to account for the effect due to the instantaneous motion of the bridge deck. At the upstream inlet boundary, a smooth and uniform velocity profile together with an additional velocity caused by the coordinate transformations is imposed. At the other penetrable boundaries (side and exit boundaries of the flow domain), zero-gradient boundary specifications with a similar treatment due to the coordinate transformations are adopted. For the pressure specifications, on the other hand, the average pressure at the downstream section of the flow domain is chosen as the reference pressure. At the other penetrable and solid boundaries, the values at the phantom cells are given according to a zero-gradient assumption in the direction normal to the boundaries.

In all cases, the domain of flow calculations is in a rectangular shape ($50D \times 30D$ with a grid size of 139×81 ; see a typical mesh system in Fig. 2). The distances between the deck and the inlet as well as the exit are respectively $14D$ and $28D$, and a space of $14.5D$ is set between the deck and the side boundaries of the flow domain. By using these selections, preliminary numerical tests have shown that the relative error of the computational results is less than 3%.

2. Calculation of Bridge Responses

In the computations of the deck motions, the dynamic equations in the vertical (across-wind) and torsional directions are respectively

$$\ddot{y}_V + 2\xi_V \omega_V \dot{y}_V + \omega_V^2 y_V = \frac{F_L}{M}, \quad (7)$$

$$\ddot{\alpha} + 2\xi_T \omega_T \dot{\alpha} + \omega_T^2 \alpha = \frac{F_M}{I}, \quad (8)$$

where \ddot{y}_V and $\ddot{\alpha}$ are the accelerations; M and I denote the mass and moment of inertia of the deck cross-section; F_L and F_M , obtained from the results of flow calculations, are respectively the instantaneous wind loads in the across-wind and torsional directions; ξ 's and ω 's are the damping ratios and circular frequencies of the deck.

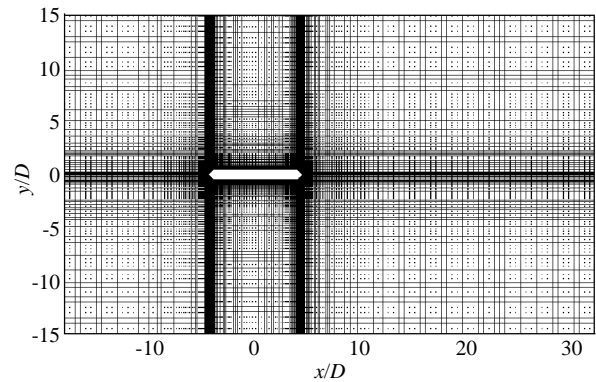


Fig. 2 Typical mesh system and domain of flow computations ($\theta = 90^\circ$)

3. Flutter Derivatives

For a 2-degree-of-freedom bridge deck, the lift and moment loads exerted on an oscillating bridge section induced by the vertical and torsional motions are given by the following equations (Scanlan and Tomko, 1971)

$$(F_L)_I = \rho U^2 B [KH_1^* \frac{\dot{y}_V}{U} + KH_2^* \frac{B\dot{\alpha}}{U} + K^2 H_3^* \alpha + K^2 H_4^* \frac{y_V}{B}], \quad (9)$$

$$(F_M)_I = \rho U^2 B^2 [KA_1^* \frac{\dot{y}_V}{U} + KA_2^* \frac{B\dot{\alpha}}{U} + K^2 A_3^* \alpha + K^2 A_4^* \frac{y_V}{B}], \quad (10)$$

where $K = 2\pi f_V B/U$; B is the deck width; H_j^* and A_j^* ($j = 1$ to 4) are the flutter derivatives.

Based on the time-series results of the numerical calculations, the flutter derivatives are obtained by the logarithmic-decrement method (Scanlan and Tomko, 1971) in the study. In addition, the initial vertical and torsional amplitudes of the bridge deck are selected respectively as $0.25D$ and 1.3° , which are considered reasonably small to avoid the amplitude effects (Noda *et al.*, 2003).

IV. EXPERIMENTAL PROGRAM

A sectional deck model is installed on a suspended rack mechanism (see Fig. 3) in the test section ($80 \text{ cm} \times 80 \text{ cm}$) of a wind tunnel. The turbulence level (intensity) of the approaching flows in the tests is less than 0.5%. The thickness (D) of the deck model is 0.04 m, corresponding to a blockage ratio of 5%. An additional energy absorber, filled with a viscous liquid, is set to produce appropriate damping in the vertical and torsional directions. Hot-film anemometry is used to measure the approaching flow

Table 2 Related properties of other experiments

	Mass (M) (kg/m)	Moment of inertia (I) (kg-m ² /m)	Fundamental frequency (Hz)		Damping ratio (%)	
			Vertical (f_v)	Torsional (f_T)	Vertical (ξ_v)	Torsional (ξ_T)
Case 1*	4.01 (Noda <i>et al.</i> , 2003)	0.0706	10.31	29.7	0.81	0.66
Case 2**	4.19 (Gu <i>et al.</i> , 2000)	0.0612	2.55	5.06	1.72	1.82
Case 3***	11.93 (Iwamoto & Fujino, 1995)	0.091	1.875	3.624	0.5	0.4

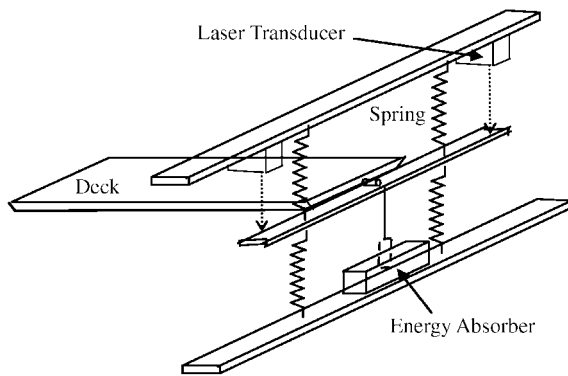
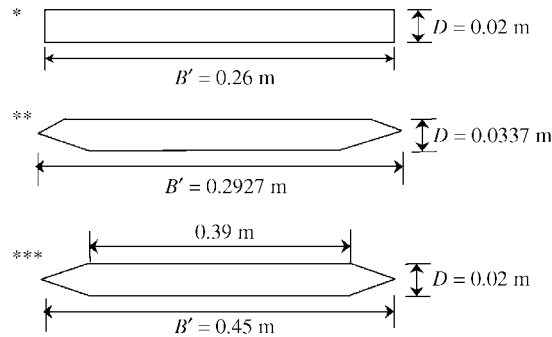


Fig. 3 Setup of section model experiments

speed. Moreover, four laser transducers are set on the rack mechanism to monitor the motion of the vibrating model deck. Other related physical quantities are illustrated in Table 1.

V. RESULTS

1. Verification of the Numerical Method

Available data from three wind tunnel measurements are selected and compared with the results from the numerical predictions. Among the selected cases, Case 1 is associated with a rectangular deck shape (Noda *et al.*, 2003); Cases 2 (Gu *et al.*, 2000) and 3 (Iwamoto and Fujino, 1995) are hexagonal cross-sections (see Table 2 for deck properties).

Compared to the experimental results from Noda *et al.* (2003), Figs. 4 show the calculated variations

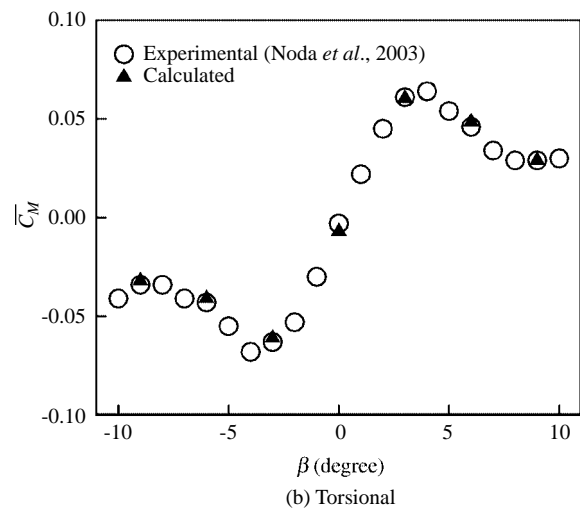
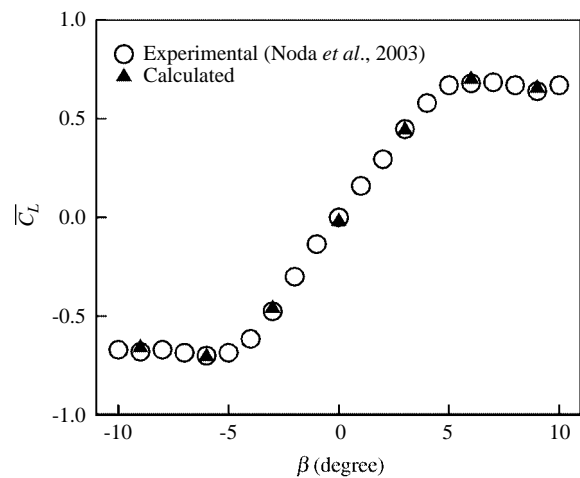


Fig. 4 Comparisons of mean force coefficients

Table 3 Comparisons of the critical flutter speed

	Critical flutter speed (m/s)		Relative error (%)
	Experimental	Calculated	
Case 2 (Gu <i>et al.</i> , 2000)	19.5	19.65	0.8
Case 3 (Iwamoto & Fujino, 1995)	16.5	16.65	0.9

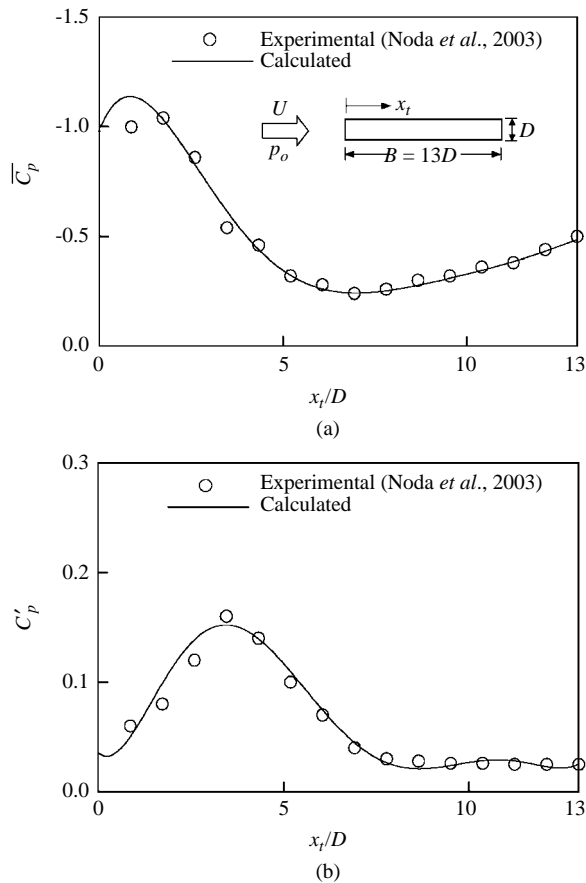


Fig. 5 Comparisons of mean and root-mean-square pressure coefficients

of normalized mean force coefficients with respect to the attack angles ($\bar{C}_L = \bar{F}_L / \rho U^2 B$ and $\bar{C}_M = \bar{F}_M / \rho U^2 B^2$; \bar{F}_L and \bar{F}_M are respectively the mean wind loads in the across-wind and torsional directions). Figs. 5 illustrate the comparisons of the normalized mean and root-mean-square pressure distributions on the upper surface of the rectangular deck ($\bar{C}_p = (p - p_o) / (0.5 \rho U^2)$ and $C_p' = p' / (0.5 \rho U^2)$; p_o is the approaching-flow pressure and p' is the root-mean-square value of local pressure). Additionally, Fig. 6 depict the comparisons of the variations of flutter derivatives.

All the results reveal that the flow effect and the resulting deck motions are well predicted. Considering the onset of flutter, on the other hand, Table 3 shows that the predicted critical flutter

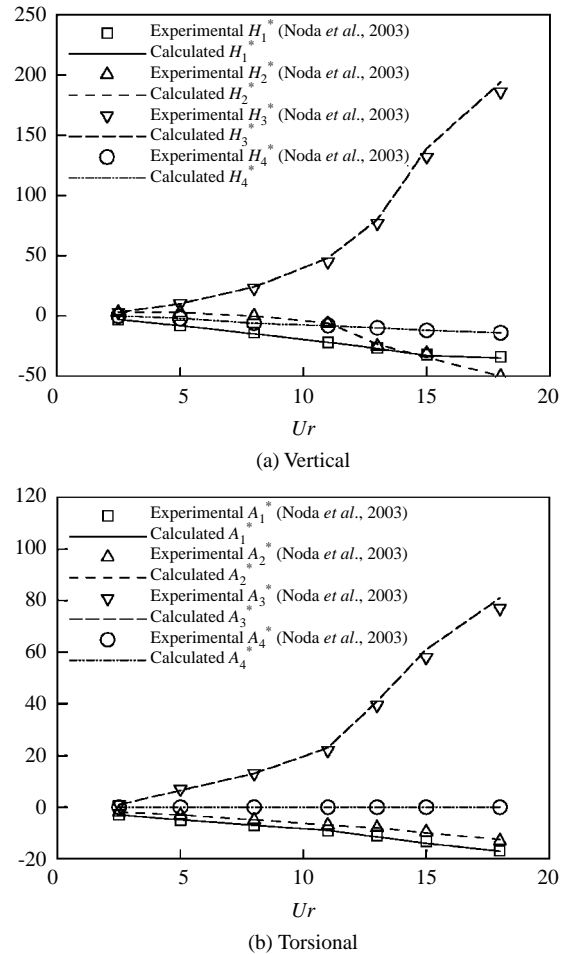


Fig. 6 Comparisons of flutter derivatives

speeds (U_{cr}) are in good agreement with those from the experiments (Gu *et al.*, 2000; Iwamoto and Fujino, 1995), indicating that the proposed numerical method is capable of predicting the deck motions with good accuracy.

2. Deck Responses

Based on the results of present wind tunnel measurements and numerical predictions, Figs. 7 to 10 show the resulting root-mean-square values of the vertical and torsional deck deflections at various approaching wind speeds. In the figures, the variations of the normalized deflections are presented in terms

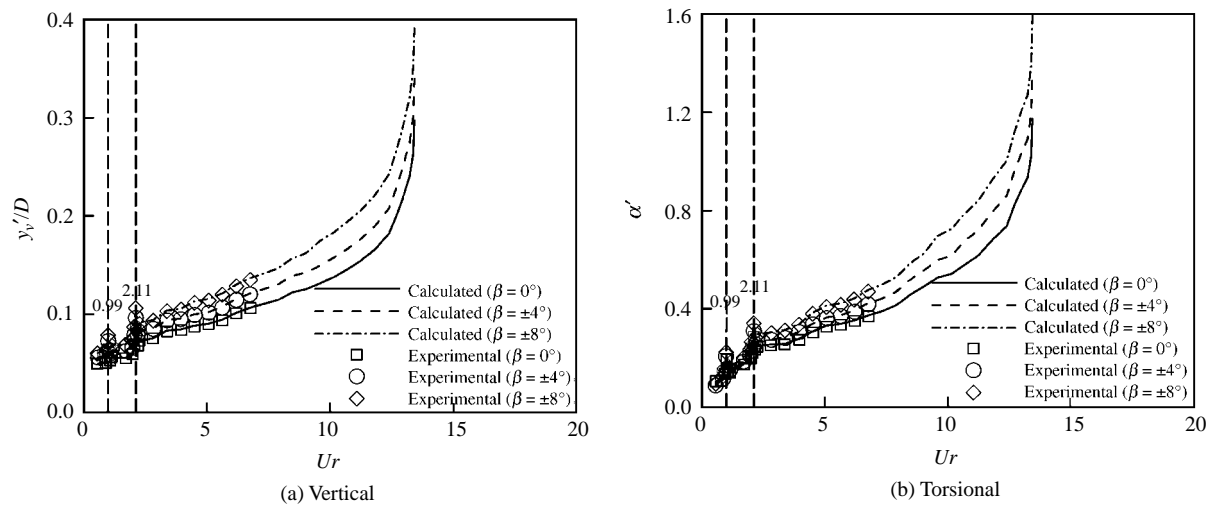


Fig. 7 Comparisons of root-mean-square deflections ($\theta = 180^\circ$)

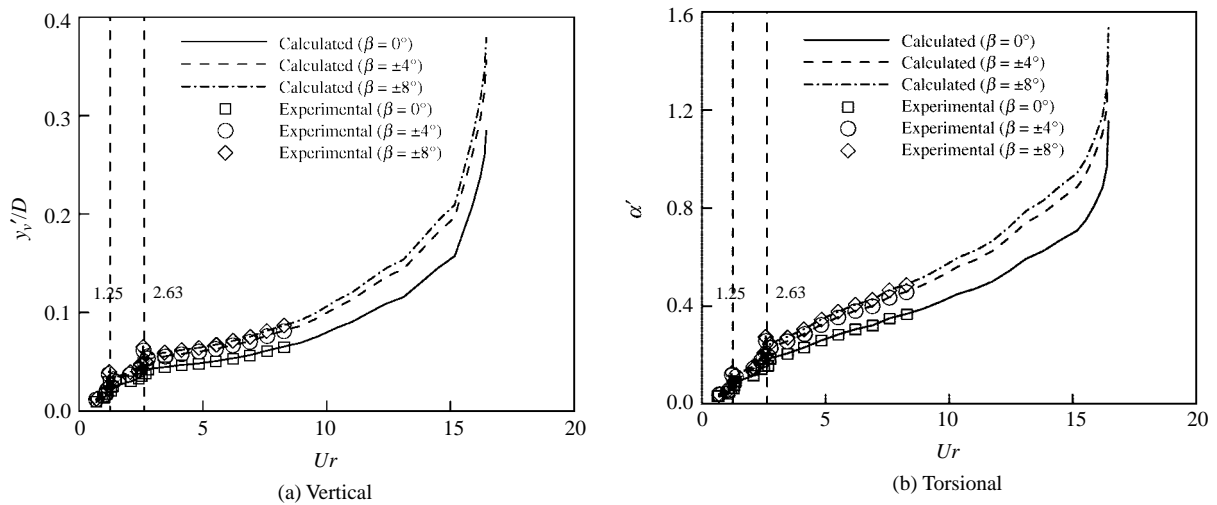


Fig. 8 Comparisons of root-mean-square deflections ($\theta = 90^\circ$)

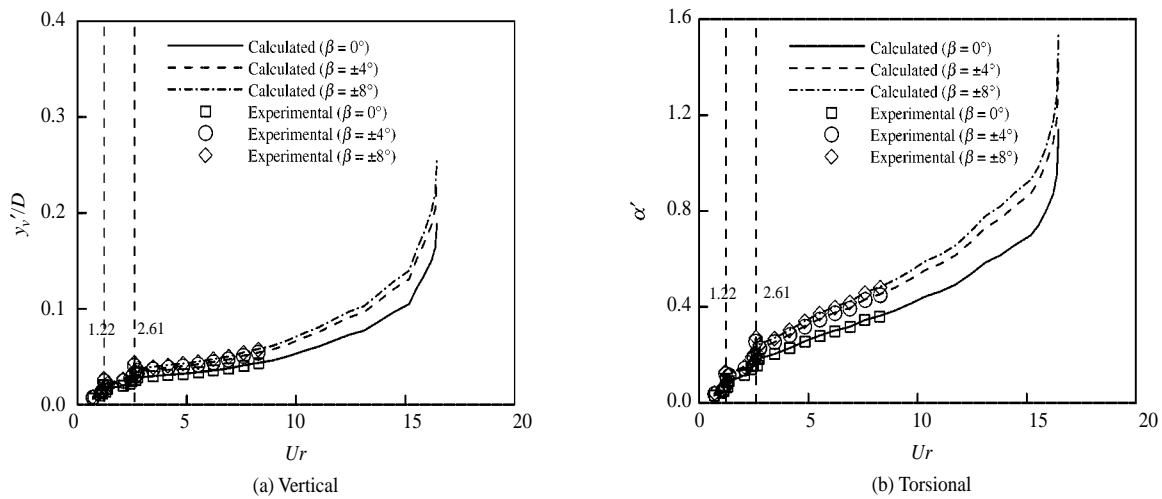


Fig. 9 Comparisons of root-mean-square deflections ($\theta = 60^\circ$)

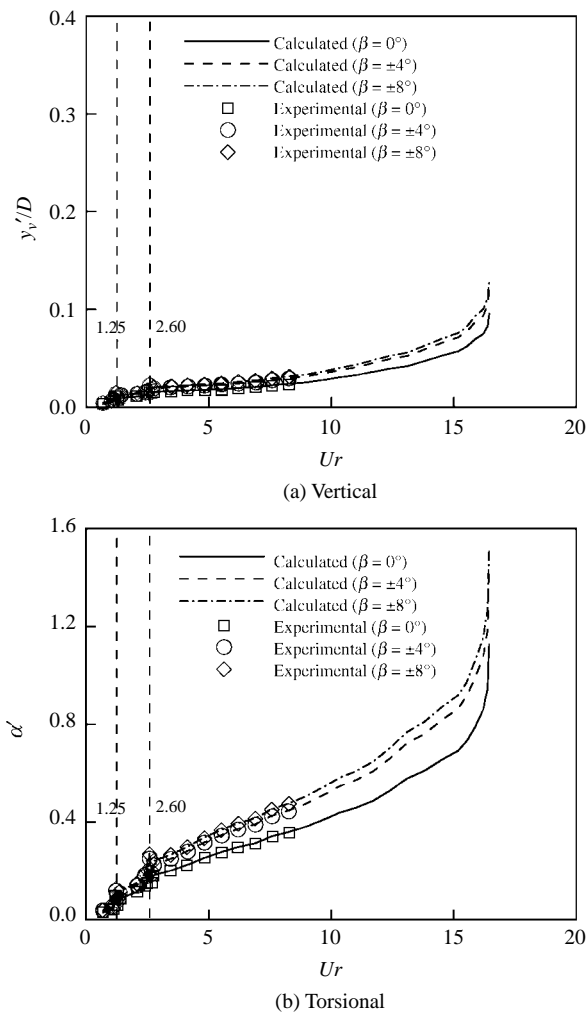


Fig. 10 Comparisons of root-mean-square deflections ($\theta = 30^\circ$)

of the reduced velocities associated with the fundamental deck frequency in the across-wind direction ($Ur = U/(f_v B)$). It can be seen that good agreements between the sets of measurement results and numerical predictions are obtained.

Generally, the root-mean-square deflections in both directions increase as the wind speed (or the reduced velocity) increases, except when two resonances occur, leading to the occurrence of local peak values. As the results of the rectangular deck ($\beta = 180^\circ$; Fig. 7) are examined, for example, situations where Ur reaches 0.99 and 2.11 correspond to the cases where shedding frequency coincides with the deck fundamental frequencies respectively in the vertical and torsional directions. To avoid damage of the deck model, unfortunately, the wind speed in the experiments is limited to about 20 m/s ($Ur = 7$). The numerical results, however, show that the normalized root-mean-square deflections increase dramatically as the reduced velocity exceeds about 13. Above this speed, numerical predictions show that the fluctuating responses in both

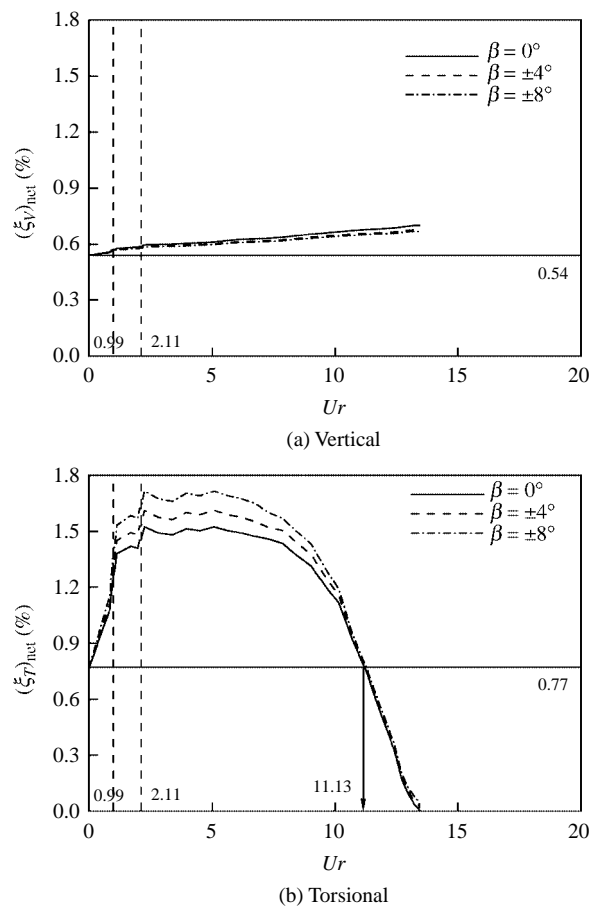


Fig. 11 Calculated net damping ratios at various wind speeds ($\theta = 180^\circ$)

directions diverge, indicating the occurrence of flutter. Moreover, among all the cases with different attack angles, the one corresponding to the largest β value ($\pm 8^\circ$) results in the greatest extent of fluctuating deflections in both the vertical and torsional directions.

Comparing to those of the rectangular deck, the variations of the root-mean-square deflections of the three hexagonal decks (see Figs. 8 to 10) have a similar tendency. However, the magnitudes of the fluctuating deflections are relatively smaller. The case when β equals $\pm 8^\circ$ still leads to the greatest normalized root-mean-square responses, and when β is equal to 0° the responses are the least. Furthermore, divergence of deflection fluctuations of the three hexagonal decks occurs apparently at larger wind speeds than that of the rectangular deck, and the normalized critical flutter speed ($V_{cr} = U_{cr}/(f_v B)$) increases with a decrease of θ .

3. Aerodynamic Damping

Based on the numerical results, Figs. 11 to 14 show the variations of the net damping ratios at various approaching wind speeds. In the case of the rectangular deck (see Fig. 11), typically, the variations

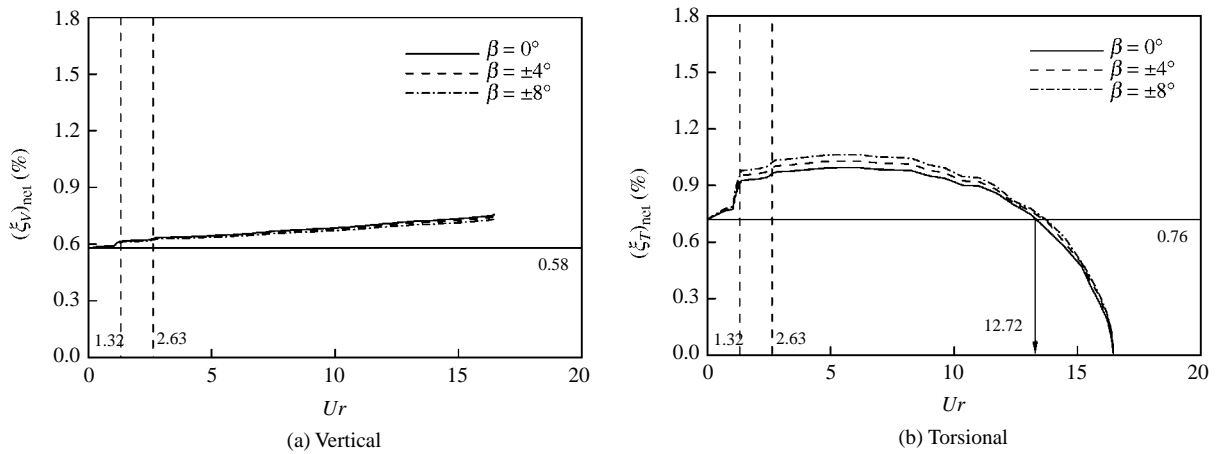


Fig. 12 Calculated net damping ratios at various wind speeds ($\theta = 90^\circ$)

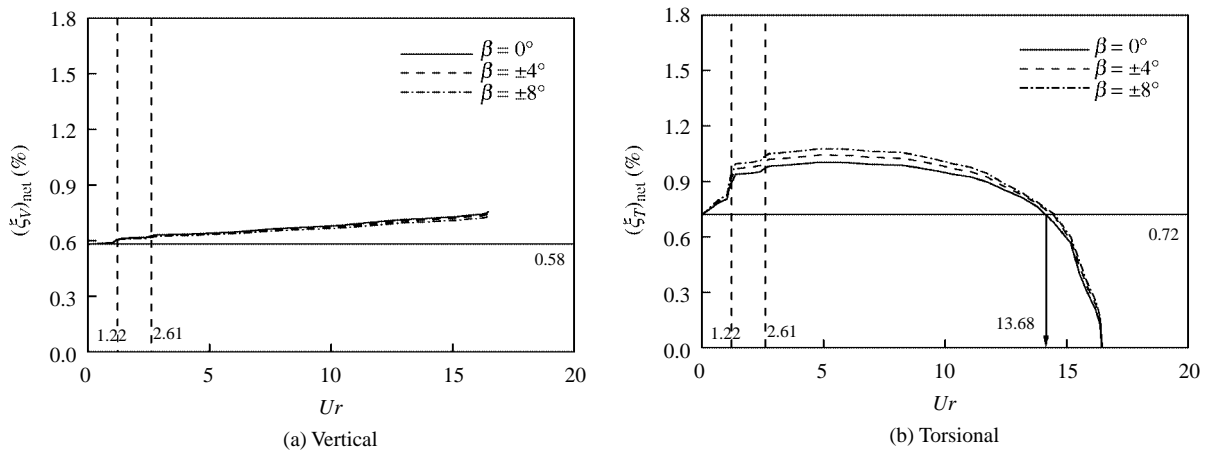


Fig. 13 Calculated net damping ratios at various wind speeds ($\theta = 60^\circ$)

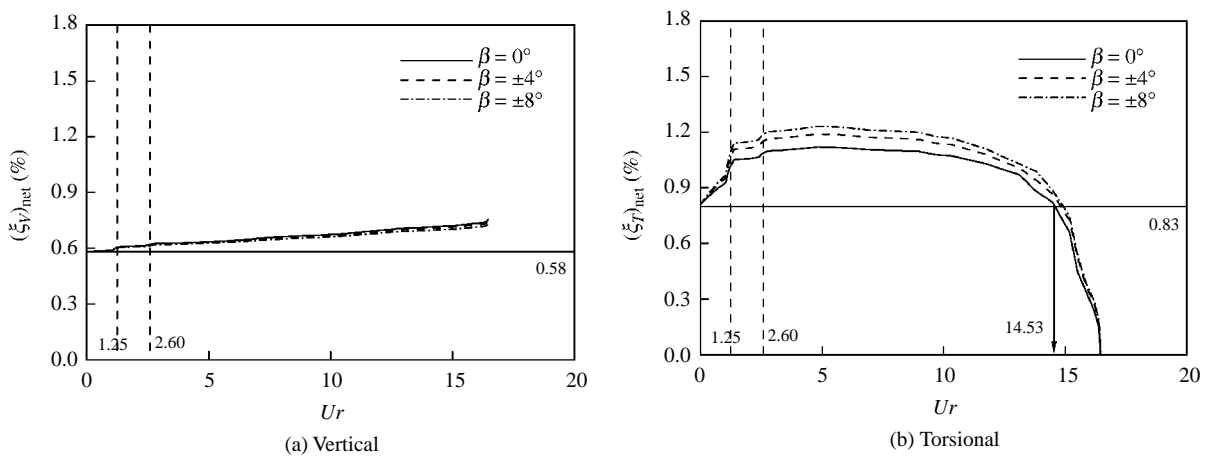
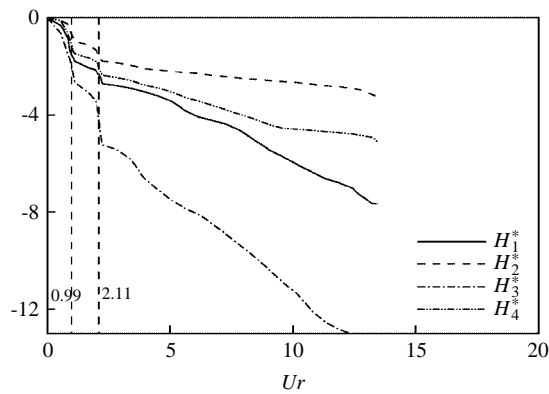


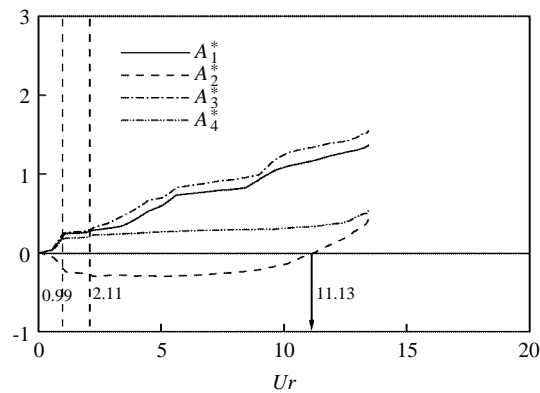
Fig. 14 Calculated net damping ratios at various wind speeds ($\theta = 30^\circ$)

of the ratios in the across-wind direction start from the value of the material damping (0.54%) then increase monotonically with an increase in wind speed. Also, the effect due to the change of β appears

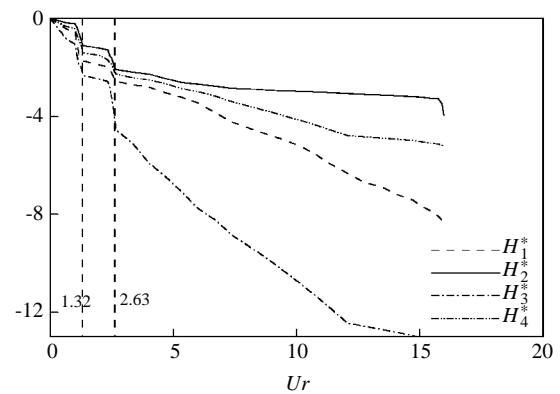
insignificant. In the torsional direction, in contrast, the variation pattern of the net damping ratios appears rather different. The damping ratio starts with the material damping value (0.77%) and increases with



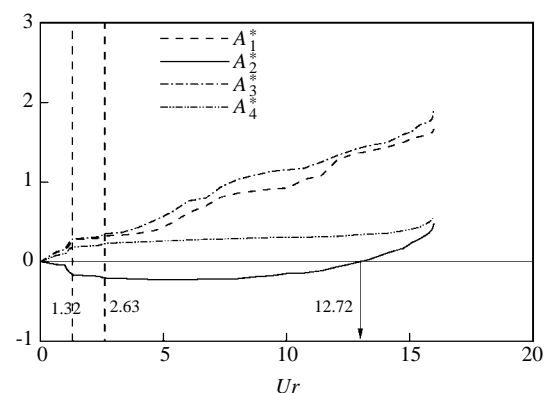
(a) Vertical



(b) Torsional

Fig. 15 Calculated flutter derivatives at various wind speeds ($\theta = 180^\circ$, $\beta = 0^\circ$)

(a) Vertical



(b) Torsional

Fig. 16 Calculated flutter derivatives at various wind speeds ($\theta = 90^\circ$, $\beta = 0^\circ$)

an increase in wind speed until Ur is about 2. After reaching a peak value, the ratio then decreases. As the reduced velocity exceeds 11.13, the net damping ratios become less than the material damping (0.77%). Finally, the ratio drops to a zero value as Ur approaches about 13. It is noticed that although the case where $\beta = \pm 8^\circ$ leads to the largest net damping ratios within a major portion of the wind speed range, the resulting normalized wind speeds corresponding to a zero net damping ratio (or the normalized critical flutter speed, V_{cr}) appear insensitive to the change of β .

For the three hexagonal decks, Figs. 12 to 14 illustrate similar tendencies of variation in the net damping ratios. In the across-wind direction, again, the net damping ratios increase monotonically with an increase in wind speed and the effect of β is mild. In the torsional direction, on the other hand, similar tendencies of the variations of the net damping ratios are found, except that the normalized flutter speeds are apparently greater than that of the rectangular deck. Besides, a smaller θ value results in a larger critical flutter speed or better aerodynamic stability performance of the deck.

4. Flutter Derivatives

Figures 15 to 18 show the variations of the flutter derivatives of all the deck cases with a zero attack angle ($\beta = 0^\circ$). It can be seen that those related to the aeroelastic forces in the across-wind direction (H_1^* to H_4^*) are all negative (Figs. 15a to 18a) within the wind speed range. In the torsional direction, on the other hand, all related derivatives are positive except the one associated with the torsional speed (A_2^*), which is initially negative at lower wind speeds then becomes positive as Ur exceeds 11.13, 12.72, 13.68 and 14.53, corresponding to cases where θ equals 180° , 90° , 60° and 30° respectively (Figs. 15b to 18b).

5. Critical Flutter Speeds

As the onset of flutter is initiated when the net damping ratio becomes zero, the critical flutter speed can be accurately evaluated based on the numerical results from Figs. 11b to 14b. Table 4 illustrates the resulting normalized critical flutter speeds (V_{cr}). It shows that in all four deck cases, the change of the attack angle (β) has a mild effect on the resulting V_{cr} .

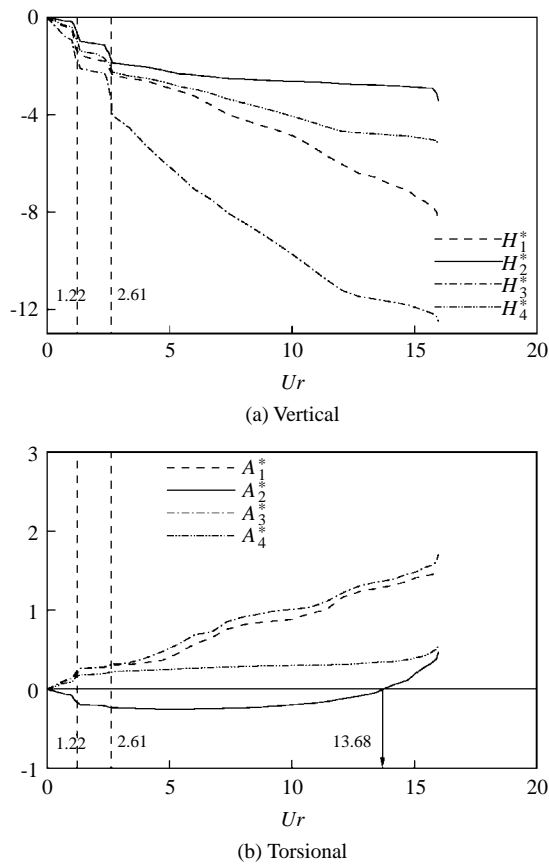


Fig. 17 Calculated flutter derivatives at various wind speeds ($\theta = 60^\circ, \beta = 0^\circ$)

values. However, the effect due to the change of θ appears significant. In particular, when θ changes from 180° (rectangular) to 90° (hexagonal), the normalized critical flutter speed increases from about 13.3 to 15.5 (about 16%), indicating a significant improvement of the deck stability. For the three hexagonal deck cases, on the other hand, a decrease of θ also leads to an increase of the V_{cr} value but to a relatively milder extent.

VI. DISCUSSION

1. Applicability and Validity of the Numerical Method

As the results from the measurements are treated as prototype data for verification, the application of the proposed numerical method has been proved to be quite successful in predicting the dynamic behaviors of the deck and the surrounding flow, which are actually interacting with each other. The variations of the root-mean-square deflections of hexagonal decks are well predicted (Figs. 4 to 7), even when resonance and flutter occur. Based on the numerical results, moreover, other important features associated

Table 4 Comparison of the normalized critical flutter speed

$\theta \backslash \beta$	180°	90°	60°	30°
0°	13.28	15.44	15.73	16.45
$\pm 4^\circ$	13.34	15.49	15.79	16.51
$\pm 8^\circ$	13.41	15.52	15.87	16.62

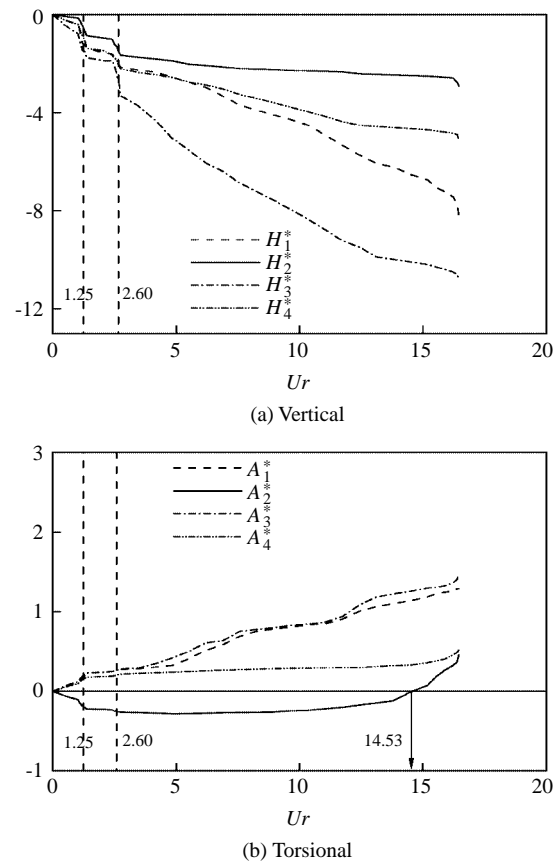


Fig. 18 Calculated flutter derivatives at various wind speeds ($\theta = 30^\circ, \beta = 0^\circ$)

with the deck motion, such as the variations of the net damping ratios and flutter derivatives as well as the critical flutter speeds, are obtained to help with the analysis of the interactive behavior between the motions of the structure and the surrounding flow.

As the present numerical method is applied to simulate the flow around the rectangular deck in the work of Noda *et al.* (2003), Fig. 5b illustrates that the surface root-mean-square pressure distribution is well simulated. However, some deviation of mean pressure is detected (Fig. 5a) in the region near the deck leading edge, where separation occurs. This inconsistency is considered owing to the error of turbulence

modeling. As the discrepancy covers solely a minor portion of the deck width, on the other hand, the good agreements in terms of the flutter derivatives (Fig. 6), critical flutter speed (Table 3) and root-mean-square deck deflections (Figs. 7 to 10) in various deck cases indicate that the validity of the present numerical method is acceptable in predicting the dynamics of the problem.

2. Advantage of Applying Numerical Computation

It commonly occurs in wind tunnel tests that the onset of flutter is sensitive to a gradual increase of the wind speed as the approaching flow velocity is near the critical flutter speed. In the present study, therefore, the wind speed is limited to about 20 m/s to avoid damage to the deck model. On the other hand, there is no such limitation when the numerical computation is performed. As long as the correctness of the present numerical methods is verified, which has just been discussed, the predicted structural responses can provide supplemental data, which allow for extensive examinations of the dynamic mechanism of the vibrating deck.

3. Mechanism of Deck Instability

In the present deck cases, the mechanism of the occurrence of flutter can be explored by examining the variations of the net damping ratios. Figs. 11a to 14a show that the resulting net damping ratio in the vertical (across-wind) mode is always larger than that of the material damping, revealing that the induced positive aerodynamic damping ratio due to the deck motion tends to suppress the vertical structure response. This evidence can also be detected by examining the corresponding H_1^* results (see Figs. 15a to 18a). As H_1^* is associated with the vertical vibrating speed (\dot{y}_v) of the deck, it represents the part of aeroelastic damping force induced by the vertical speed of the deck motion. Since H_1^* is negative throughout the entire wind speed range, the resulting negative aeroelastic force then indicates a decrease of the total vertical force and also a decrease of the deck response in the vertical direction. Moreover, as this negative induced damping force can be represented in a form of $(c_a \dot{y}_v)$; c_a denotes the aerodynamic damping ratio) and is moved to the left-hand-side of the dynamic equation of the vertical deck motion, it ends up with an increase of the total damping ratio. The outcome of the deduction from the results in Figs. 15a to 18a agrees with those shown in Figs. 11a to 14a.

By examining the results from Figs. 15b to 18b, on the other hand, it can be seen that the net damping ratios in the rotational (torsional) mode drop to zero at the critical flutter speeds. Accordingly, one can then conclude that although the fluctuating responses diverge in both directions at the critical flutter speeds

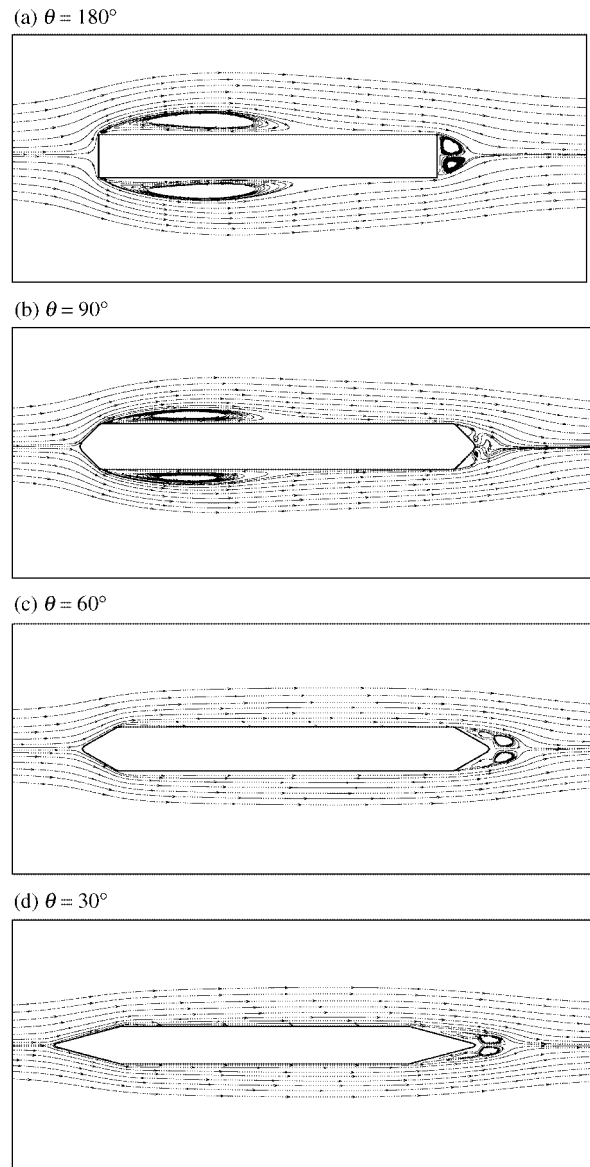


Fig. 19 Calculated mean streamline patterns of fixed decks ($\beta = 0^\circ$)

(Figs. 7 to 10), the instability of all the decks is in reality subject to torsional flutter. It is also noted that when the net torsional damping ratio becomes identical to that of the material damping (Figs. 7b to 10b), A_2^* changes its sign (Figs. 15b to 18b). All these evidences can be clearly found by investigating the results from the numerical computations.

4. Effect of Side Angles

Finally, the reason why a decrease of θ tends to improve the aerodynamic instability of the deck can be found by investigating the surrounding flow behavior. Based on the numerical results, Figs. 19 and 20 show the mean flow streamlines around a fixed

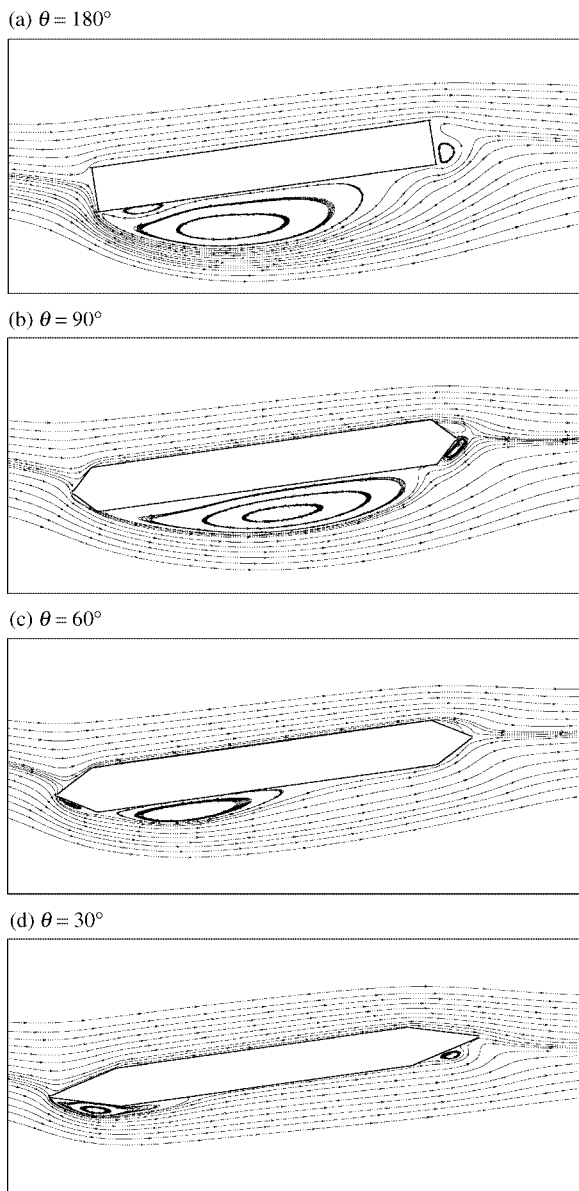


Fig. 20 Calculated mean streamline patterns of fixed decks ($\beta = 8^\circ$)

deck with various θ values typically when the attack angle (β) is equal to 0° and 8° . In the cases of a zero attack angle (see Fig. 19), one can see that as θ decreases the size of the re-circulating flow near the deck surfaces tends to diminish. When β is equal to 8° , although separation bubbles are produced on one (lower) side of the deck, a similar tendency is obtained (see Fig. 20). Physically, the area of the separation bubble in the mean flow indicates the region of instantaneous unsteady flow. Accordingly, as the side angle (θ) decreases, the shape of the deck becomes more streamwise, leading to a decrease of the extent of flow unsteadiness. Consequently, the resulting fluctuating wind forces also decrease (see Table 5) and lead to less significant structure responses.

Table 5 Comparison of the calculated root-mean-square forces and moments

$\theta \backslash \beta$		θ			
		180°	90°	60°	30°
0°	C_L'	0.1518	0.0793	0.0245	0.0101
	C_M'	0.0634	0.0349	0.0129	0.0067
8°	C_L'	0.2207	0.1298	0.0704	0.0419
	C_M'	0.1068	0.0546	0.0228	0.0104

5. Comparison of Deck Instability

Among the cases in the present study, it is shown in Table 4 that the resulting normalized critical flutter speed (V_{cr}), indicative of the onset of torsional divergence, increases with a decrease of the side angle (θ) at all the attack angles. It is important to point out that the case with a zero side angle corresponds to a rectangular deck, whose critical flutter speed is apparently lower (about 16%) than those in the three hexagonal deck cases. This implies that a hexagonal deck generally possesses much better stability performance than a rectangular one. On the other hand, as θ decreases from 90° to 30° in the three hexagonal deck cases, the critical flutter speed decreases about 7% (also see Table 4). This reveals that a decrease of the side angle (θ) tends to improve the deck instability but to a relatively milder extent.

VII. CONCLUSIONS

The interaction between a suspension bridge with a hexagonal cross-section and the surrounding flow has been extensively examined by adopting numerical computations. After comparison with wind tunnel results and other available experimental results, the proposed numerical model has been proved to be adequate in predicting wind effects as well as the dynamic behavior of the deck with good accuracy. Finally, it is found that a hexagonal deck possesses much better stability performance than a rectangular one. In terms of the critical flutter speed, the increase can be on the order of 16%. Moreover, for a hexagonal deck, a decrease of the side angle (θ) tends to improve the deck stability but to a relatively milder extent.

ACKNOWLEDGMENTS

The study is cordially funded by the National Science Council in Taiwan (grant No. NSC 92-2211-E-005-028 and NSC 93-2211-E-005-008).

NOMENCLATURE

B width of upper surface of deck

B'	maximum width of deck
c_a	Aerodynamic damping
\bar{C}_L, \bar{C}_M	mean lift and moment coefficients
C_L', C_M'	Root-mean-square lift and moment coefficients
\bar{C}_p, C_p'	mean and root-mean-square pressure coefficients
D	deck thickness
F_L, F_M	wind loads in the across-wind and torsional directions
f_V, f_T	fundamental frequencies of deck in the across-wind and torsional directions
H_j^*, A_j^*	flutter derivatives
I	moment of inertia of deck
K	$2\pi f_V B/U$
k	bulk modulus of elasticity
M	mass of deck
p	pressure
U_o	approaching-flow speed
Ur	$U/(f_V B)$; reduced velocity
U_{cr}	critical flutter speed
V_{cr}	$U_{cr}/(f_V B)$; normalized critical flutter speed
u, v	velocity components
X, Y	moving spatial coordinates
x, y	original spatial coordinates
y_V	deck deflection in the across-wind direction
\dot{y}_V	speed of deck vibration in the across-wind direction
\ddot{y}_V	acceleration of deck vibration in the across-wind direction
y_V'	root-mean-square deck deflection in the across-wind direction
α	deck deflection in the torsional direction
y_T	speed of deck vibration in the torsional direction
$\ddot{\alpha}$	acceleration of deck vibration in the torsional direction
α'	root-mean-square deck deflection in the torsional direction
β	attack angle
θ	inclined angle of deck side surfaces
ρ	fluid density
ω_V, ω_T	circular frequencies
ξ_V, ξ_T	material damping ratios
$(\xi_V)_{net}, (\xi_T)_{net}$	net damping ratios
ν, ν_t	absolute and turbulent viscosities

REFERENCES

- Courant, R., Friedrichs, K. O., and Lewy, H., 1967, "On the Partial Difference Equations of Mathematical Physics," *IBM Journal*, Vol. 11, pp. 215-234.
- Fang, F. M., Li, Y. C., Chen, C. C., Chen, J. H., and Ueng, J. M., 2001, "Dynamic Responses of a Suspension Bridge with a Rectangular Cross-Section," *Proceedings of the Fifth Asia-Pacific Symposium on Wind Engineering*, Kyoto, Japan, pp. 397-400.
- Fang, F. M., Li, Y. C., Chen, C. C., Liang, T. C., and Chen, J. H., 2005, "Numerical Predictions on the Dynamic Response of a Suspension Bridge with a Trapezoidal Cross-Section," *Journal of the Chinese Institute of Engineers*, Vol. 28, No. 2, pp. 281-291.
- Germano, M., Piomelli, U., Moin, P., and Cabot, W. H., 1991, "A Dynamic Subgrid-Scale Eddy Viscosity Model," *Physics of Fluids*, Vol. 3, pp. 1760-1765.
- Gu, M., Zhang, R., and Xiang, H., 2000, "Identification of Flutter Derivatives of Bridge Decks," *Journal of Wind Engineering and Industrial Aerodynamics*, Vol. 84, pp. 151-162.
- Iwamoto, M., and Fujino, Y., 1995, "Identification of Flutter Derivatives of Bridge Deck from Free Vibration Data," *Journal of Wind Engineering and Industrial Aerodynamics*, Vol. 54/55, pp. 55-63.
- Kuroda, S., 1997, "Numerical Simulation of Flow Around a Box Girder of a Long Span Suspension Bridge," *Journal of Wind Engineering and Industrial Aerodynamics*, Vol. 67/68, pp. 239-252.
- Lee, S., Lee, J. S., and Kim, J. D., 1997, "Prediction of Vortex-Induced Wind Loading on Long-Span Bridge," *Journal of Wind Engineering and Industrial Aerodynamics*, Vol. 67/68, pp. 267-278.
- Noda, M., Utsunomiya, H., Nagao, F., Kanda, M., and Shiraishi, N., 2003, "Effects of Oscillation Amplitude on Aerodynamic Derivatives," *Journal of Wind Engineering and Industrial Aerodynamics*, Vol. 91, pp. 101-111.
- Sarkar, P. P., Jones, N. P., and Scanlan, R. H., 1992, "System Identification for Estimation of Flutter Derivatives," *Journal of Wind Engineering and Industrial Aerodynamics*, Vol. 41-44, 1243-1254.
- Scanlan, R. H., and Tomko, J. J., 1971 "Airfoil and Bridge Deck Flutter Derivatives," *Journal of Engineering, Mechanics Division*, Vol. 97, pp. 1717-1737.
- Song, C. C. S., and Yuan, M., 1988, "A Weakly Compressible Flow Model and Rapid Convergence Methods," *Journal of Fluids Engineering*, Vol. 110, No. 4, pp. 441-455.

Manuscript Received: Mar. 27, 2006

Revision Received: May 22, 2007

and Accepted: Jun. 24, 2007